Astronomical near-neighbor detection with a four-quadrant phase mask (FQPM) coronagraph

Pierre Haguenauer, Eugene Serabyn, Bertrand Mennesson, James K. Wallace, Robert O. Gappinger, Mitchell Troy, Eric E. Bloemhof, Jim Moore, and Chris D. Koresko

Jet Propulsion Laboratory, California Institute of Technology, 4800 Oak Grove Drive, Pasadena, CA 91109, USA

ABSTRACT

Direct detection of planets around nearby stars requires the development of high-contrast imaging techniques, because of their very different respective fluxes. We thus investigated the innovative coronagraphic approach based on the use of a four-quadrant phase mask (FQPM). Simulations showed that, combined with high-level wavefront correction on an unobscured off-axis section of a large telescope, this method allows high-contrast imaging very close to stars, with detection capability superior to that of a traditional coronagraph. A FQPM instrument was thus built to test the feasibility of near-neighbor observations with our new off-axis approach on a ground-based telescope. In June 2005, we deployed our instrument to the Palomar 200-inch telescope, using existing facilities as much as possible for rapid implementation. In these initial observations, using data processing techniques specific to FQPM coronagraphs, we reached extinction levels of the order of 200:1. Here we discuss our simulations and on-sky results obtained so far.

Keywords: Coronagraphy, phase mask.

1. INTRODUCTION

In the exciting scientific goal of direct exoplanet detection, very high rejection levels are needed, imposed by the contrast between the planet and its parent star. This has led to the development of new measurement techniques, for imaging of faint companions close to a much brighter star requires being capable of observing with high contrast ratio (ratio of the flux of the bright parent star to the flux of the fainter companion) at small inner working distance (IWD). Considering "classical" Lyot[1] coronagraph techniques (use of an opaque disk to block the on-axis light), practical issues such as large IWDs limit the performances. Of course, diffracted and scattered light limit all coronagraphs to varying extents. Different novel approaches are thus being studied to overcome these limitations.[2–10]

This led us to implement a novel high-contrast coronagraph to allow for detection in the immediate vicinity of bright stars. This coronagraphic method uses a Four-Quadrant Phase Mask[3,11–14] (FQPM) in place of the opaque disk in a classical coronagraph. Specific numerical simulations have bee conducted to determine the best configuration to be used with this new type of masks. They showed that such a mask used in conjunction with an off-axis section of the telescope and high Strehl ratios, would ensure high rejection in the very close neighborhood of stars (ratio of the flux of a bright star without the coronagraph in place to the remaining flux for the same star with the coronagraph in place).

2. WHY USING A FQPM?

2.1. FQPM principle

Fig. 1 presents the working principle of a coronagraph using a four-quadrant phase mask (FQPM). The collimated beam coming from the telescope, i.e. a round and uniform pupil without central obscuration here (a), is focused on the mask (c). There, instead of affecting the intensity of the image as a classical Lyot coronagraph would do, a FQPM will change the phase of the beam. The mask is thus transparent, but splits the image plane in four

Further author information: (Send correspondence to P. Haguenauer)
E-mail: phaguena@eso.org, Telephone: +56 55 43 5262

Space Telescopes and Instrumentation I: Optical, Infrared, and Millimeter,
edited by John C. Mather, Howard A. MacEwen, Mattheus W.M. de Graauw,
Proc. of SPIE Vol. 6265, 62651G, (2006) · 0277-786X/06/$15 · doi: 10.1117/12.672595

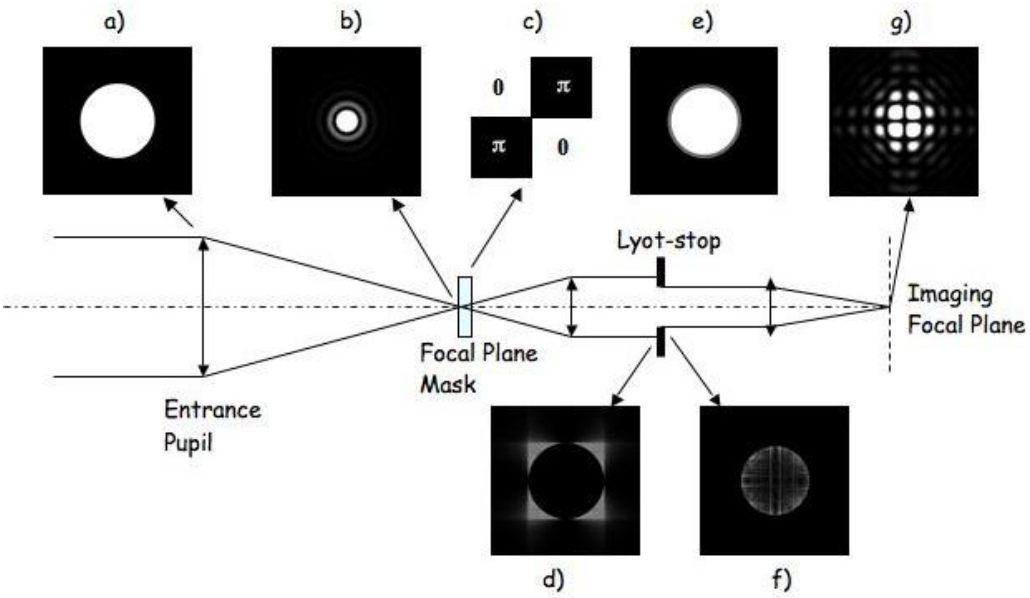

Figure 1. Four Quadrant Phase Mask principle (pixels scales have been adjusted for each image for better clarity).

quadrants and adds a phase-shift of π for two of them diametrically opposed on a diagonal. This specific design has the advantage of being geometrically achromatic. The Airy disk (b), i.e. the Fourier transform of the pupil, is focused at the exact crosshair of the mask. A second lens is then used to re-collimate the beam, also achieving a Fourier transform of the electric field. The effect of the mask then appear in the new repartition of the light in the next pupil plane (d): all the light is now concentrated on four identical sections around the original pupil which is now seen as dark. A Lyot stop (e), slightly undersized compared to the initial pupil dimension allows then to get rid of all the light and allows keeping only the central dark part (f). The new electric field can then be focused on the detector for image recording. For a star on the axis of the telescope, the pattern specific to a FQPM is then observed (g), with now a dark center on the image and a flux level much lower than the initial Airy pattern.

Fig. 2 presents the point spread functions (PSF) obtained with different cases of coronagraph. 2D images are represented as well as cuts along a diagonal of the images. As a reference, the case without any mask, i.e. an Airy disk, has been represented (solid line on the graph). Different type of coronagraph have then been used and the image obtained in the focal plane of the detector normalized to the "no-mask" case. A Lyot stop with a diameter equal to 90% of the initial pupil has been used in all cases. As can be seen on the figure, with a FQPM (_ _ line), the brightest remaining lobes are at a level close to 10^{-6} and the flux even drops to very low levels in the center of the image. For the classical Lyot coronagraph cases, the results with different diameters of the intensity occulting mask are shown. Even with a diameter of eight times the diffraction limit ($8 * \lambda/D$), the flux in the image only drops by a factor of 10^4 (_ .. _ line). One should also see here that the diameter of the mask imposes a limit on how close to the central object one will be able to observe.

2.2. Central obscuration effect

In the preceding section, we have assumed that no central obscuration was present in the telescope pupil and shown the corresponding performances of a FQPM. As we will show here, this assumption has an importance. On fig. 3 are presented the same steps on the image formation through the coronagraph as in fig. 1. As one can clearly see here, in the pupil plane just before the Lyot stop, the effect of the central obscuration is to keep some light inside the pupil. The same four spots pattern is present around the edge of the pupil and around the central obscuration, i.e. inside the pupil this time. Using a Lyot stop with a circular shape will then not allow to block all the light. Lyot stops with more complicated shapes, adapted to this specific new pattern can be used

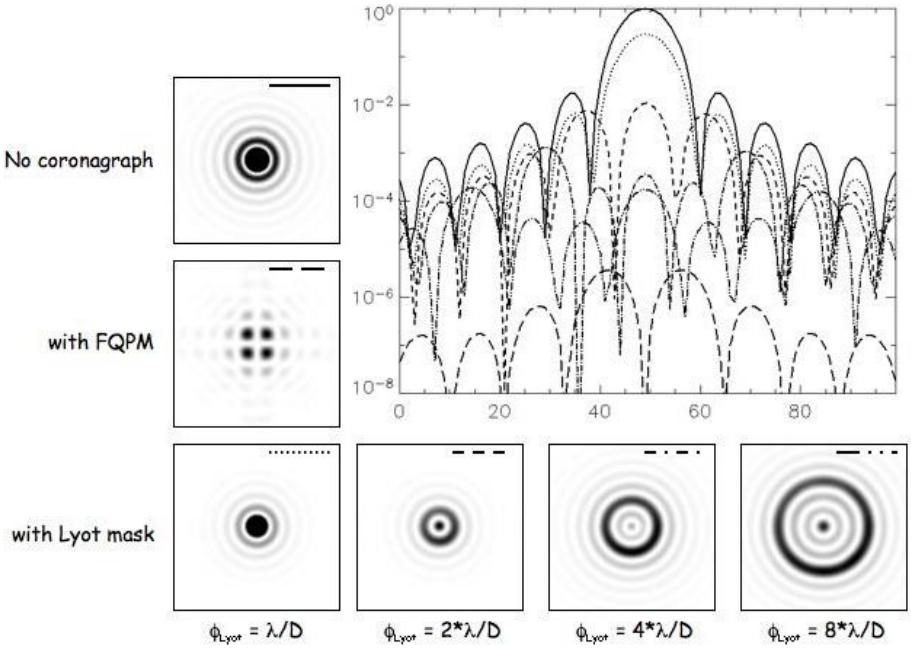

Figure 2. Point Spread Functions for different cases: Airy disk, with a FQPM, and with a classical Lyot coronagraph with different sizes for the occulting mask.

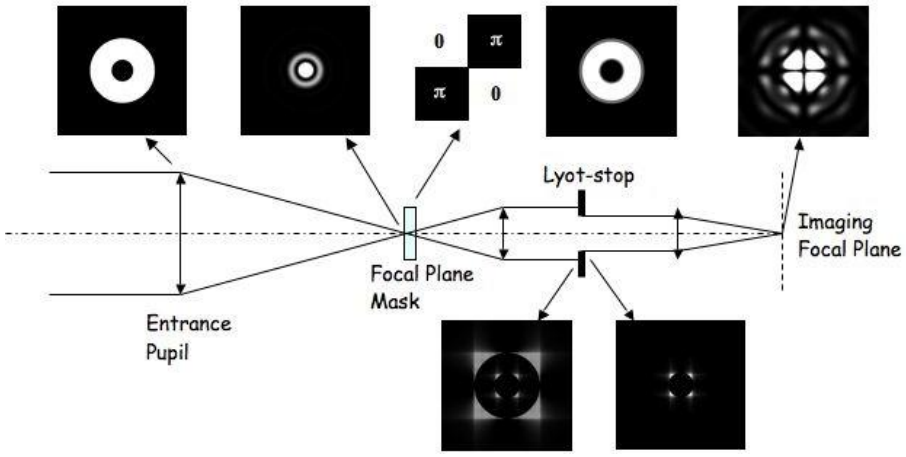

Figure 3. Effect of the central obscuration on the FQPM performances.

but their design is more complicated and they should be carefully aligned according to the system geometry. With a circular Lyot stop, the light can not be perfectly canceled and increases the level of the four center lobes on the image in the detector focal plane.

2.3. Tip-tilt effect

With a FQPM, the image has to be centered on the crosshair of the quadrants in order to cancel the on-axis light. The naturally arising question is to what precision should it be centered. In order to assess this point, we have simulated the effect of a mis-centering of the image, i.e. tip-tilt on the beam or telescope pointing error. Fig. 4 presents the results of these simulations. The image has been focused on the mask at different positions along a line at 45 degrees along one quadrant (the arrow on the quadrant image shows the direction of the centering

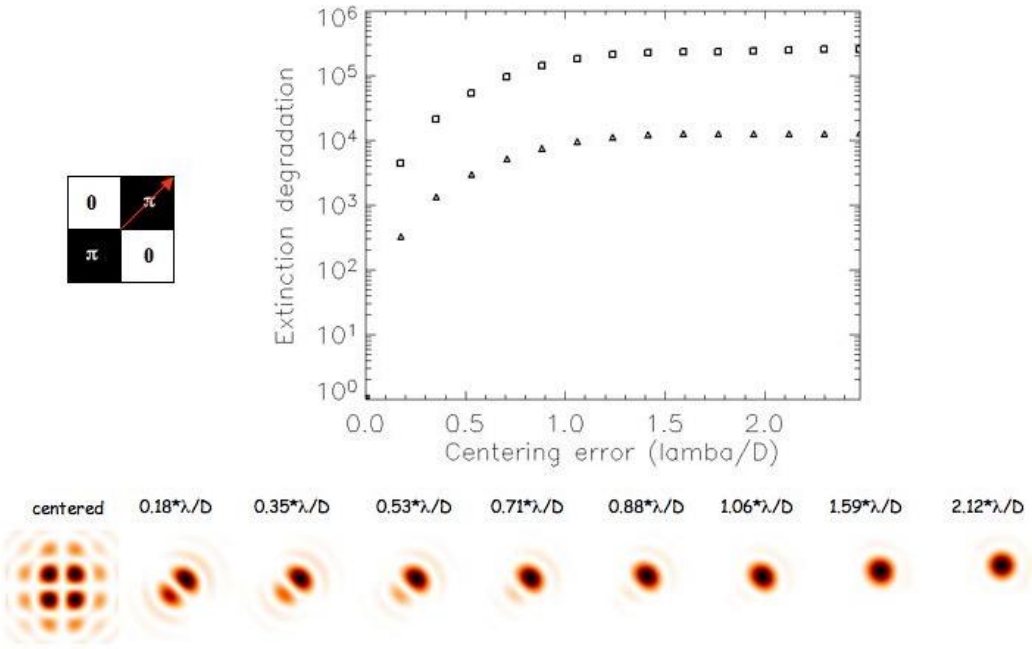

Figure 4. Effect of tip-tilt on the FQPM performances.

displacement). A 45 degrees line has been chosen as it represents the most unfavorable case. A two-quadrants phase mask also allows for some extinction (at a much lower level than a FQPM) for a beam falling on the separation between the two quadrants. So, if the mis-centering occurs along one of the separation between two of the quadrants of a FQPM, the performance decrease will be less important.

At the bottom of fig. 4 are given the images obtained in the imaging focal plane together with the corresponding shift of the image with respect to the FQPM crosshair. The image mis-centering is given in units of the telescope diffraction limit, i.e λ/D. The graphic presents the corresponding degradation of the extinction, compared to the case of a perfectly centered image, for the sum of the total energy in the image (triangles) and for the max of the image (rectangles). As one can see, even with a small displacement of $0.18 \times \lambda/D$, the extinction level will be strongly degraded. This shows that if high level of extinction can be obtained for an on-axis object, the image has to be very precisely maintained at the center of the FQPM. But the fact that the extinction level rapidly decrease when going away from the FQPM crosshair also plays as a big advantage of FQPM coronagraph compared to classical Lyot ones. At one λ/D, almost no extinction will occur, allowing thus for detection of companions or structures in the very close neighborhood of the object.

3. FQPM INSTRUMENT ON PALOMAR

As the simulations showed the innovative and powerful concept of the FQPM as an off-axis coronagraph, we developed an instrument to be taken to the telescope. Our first coronagraphic phase-masks using the four quadrants technique have been successfully manufactured at JPL and were tested with a dedicated laboratory testbench, with rejections as high as 2260:1.[15] The current design of the masks is optimized for one particular wavelength, but allows for operation in moderately wide wavelength bands with moderate performance. Future efforts will involve increasing the maximum rejection ratio and broadening the band.

The results of the simulation presented in the preceding section show that, in order to take full advantage of a FQPM performances, the following requirements have to be fulfilled for an on-sky instrument:

1. use an unobscured aperture, and

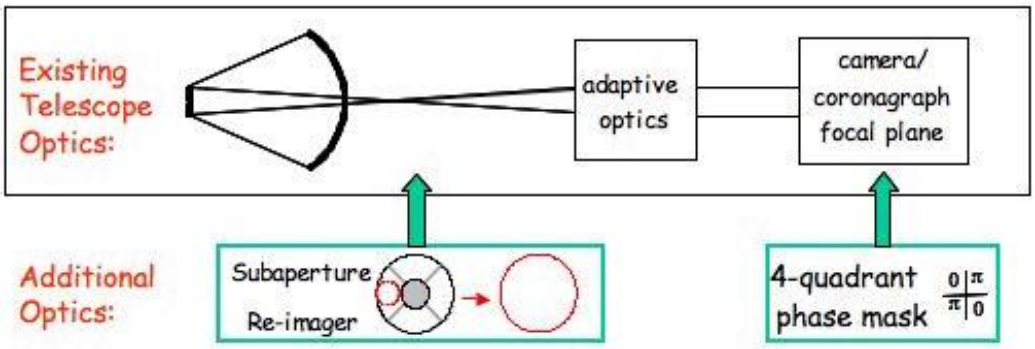

Figure 5. Implementation of the FQPM experiment on the Palomar 200-inches telescope.

2. get a high Strehl ratio.

These were thus the two guiding rules when designing our coronagraph.[16] Fig. 5 presents the concept of the instrument that was developed for the 200-inches telescope at Mount Palomar. The choice of this telescope has been driven by its large diameter, its already performant adaptive optics (AO) system, and the existence of a camera with a coronagraph focal plane (PALAO instrument[17]). Our mask could then be easily added to the camera, but one still had to find a solution to the two preceding rules. This was achieved with a very simple idea: getting a unobscured off-axis subaperture on the telescope pupil. The large diameter of the telescope allowed there to have a subaperture as big as 1.5 m. A simple optical re-imager allows then to intercept the beam, expand the pupil and send the beam back to the AO system as if it was the full pupil. One could thus benefit of very high level of correction of the atmospheric turbulence on an unobscured pupil. The beam then simply continues its path to the coronagraph and camera.

4. ON-SKY RESULTS

4.1. Strehl measurements

As it was obvious from the simulations that a high level of correction of the atmosphere was necessary to allow for good rejection, we were particularly interested in knowing the Strehl ratio (SR) that was achieved on sky, i.e. the ratio of the max of an image obtained on-sky to the max of a perfect image. We thus also recorded images through our instrument without using the mask (these images were also used for calibration of the extinction level). The Strehl ratio on these images was then computed using the following procedure:

- The centroid of the sky image is computed.
- A perfect Airy pattern is generated, with the same centroid position and the same pixel sampling as the sky image. The arcsec/pixel scale is given by the magnification of our relay optics.
- The correct angular dimension of the generated Airy is checked by the matching of the Airy rings positions between the simulated image and the sky ones.
- The total energy of both sky and perfect Airy images are normalized to one.
- The SR is calculated by taking the ratio of their max after normalization.

Fig. 6 presents the results of this method on a single star, HD121107. The left image corresponds to a single exposure of 1.416s, and the one in the center to the sum of 20 images for a total integration time of 28.32s. The images are presented in log scale for better view. The very good correction can be seen through the presence of many rings around the central spot. On the summed image, one can even see up to the ninth ring. The graph represents cuts of the short exposure (solid line) and of the perfect Airy pattern (dashed line). The SR is

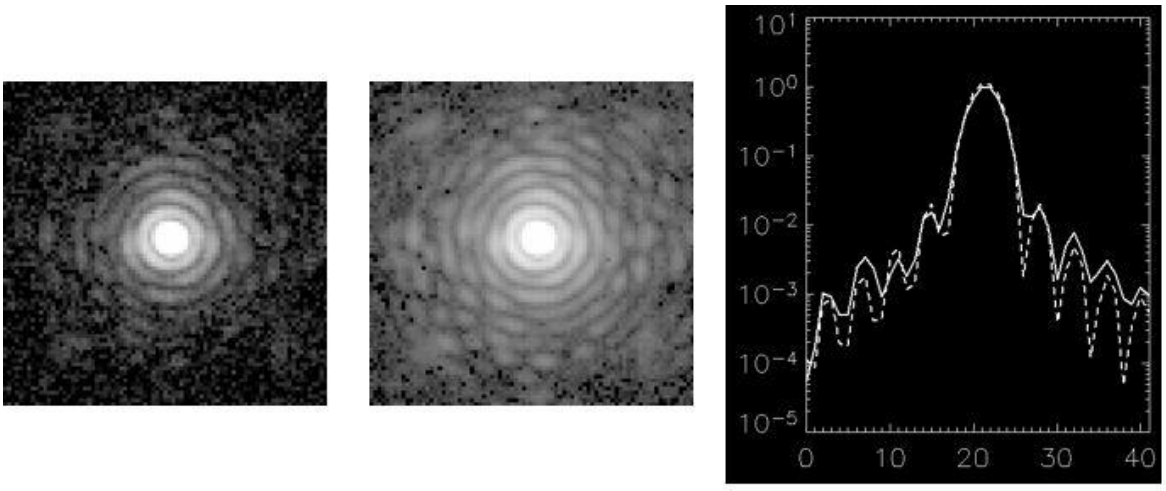

Figure 6. On-sky PSF through the FQPM coronagraph.Left: one short exposure, center: sum of twenty exposures, right: cuts along the one-exposure image (solid line) and along a reference Airy pattern (dashed line).

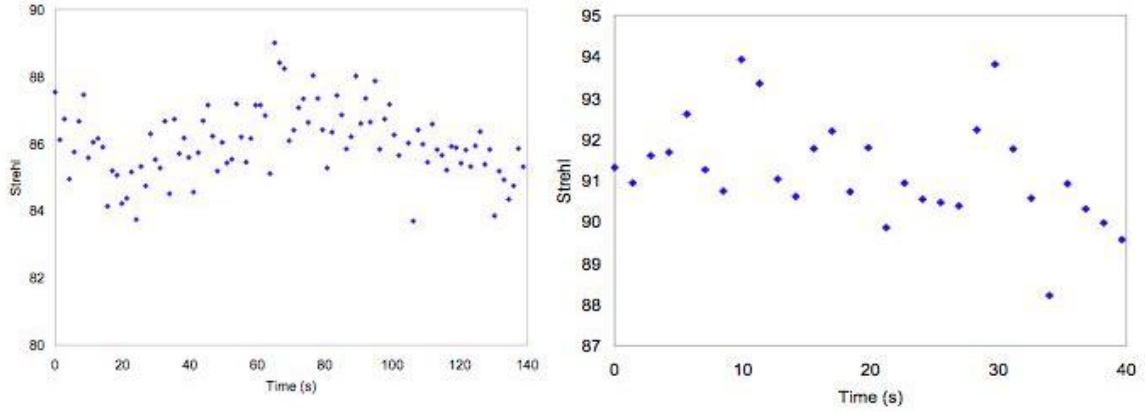

Figure 7. SR measurements versus time. Left: Alpha Boo, 06/13/2005, 100 consecutive exposures. Right: HD121107, 06/14/2005, 29 consecutive exposures.

computed as the ratio of the max of these two cuts. Strehl ratios as high as 94% have been obtained, during an observing run of three nights in June 2005.

Fig. 7 presents some results of obtained SR versus time, on two different objects and for two consecutive nights. The left graph presents the SR computed on 100 exposures of 1.416s each, on Alpha Boo on the night of June 13th 2005. The average of the SR is of 85.9% here with a standard deviation of 1.4%. The right graph presents the same kind of results for 29 exposures of 1.416s each, on HD121107 on the night of June 14th 2005, and shows the best achieved SR during the observing run. The average of the SR is of 91.2% here with a standard deviation of 1.2%. Measuring the SR on all the calibrating data during the three nights allowed us to assess the short and long time evolution of the quality of the wavefront correction. The small standard deviation of the measured SR on a batch of images shows the very good short time stability of the correction. SR at the level of 80% were routinely obtained showing the good long time stability of the system.

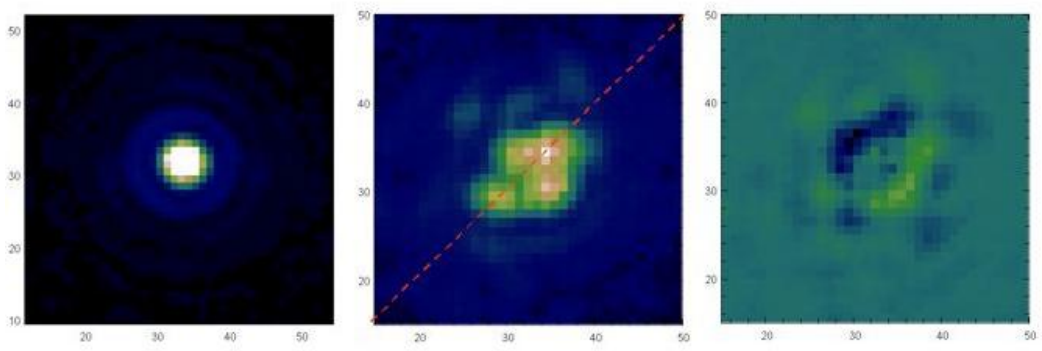

Figure 8. Image of a single star (HD121107) through the FQPM instrument. Left: image obtained off the mask (off-FQPM). Center: with the star centered on the crosshair of the mask (on-FQPM). Right: on-FQPM image after data processing using quadrants subtraction.

4.2. Extinction measurement

The first on-sky test of our FQPM instrument was conducted during the nights of June 13^{th} to 15^{th} 2005. On fig. 8 and fig. 9, one can see some results obtained during this first observing run. Fig. 8 shows the first on-sky images of the FQPM, with our magnified system, in the narrowband $Brackett - \gamma$ filter. These images were obtained on a single star, HD121107. The left-hand image corresponds to the image of the star when the light was going through our system but simply through one quadrant, i.e without being affected by the mask. Images like this one were taken on all targets to be used as calibration of the extinction. The center image corresponds to the case where the stellar image is centered on the quadrant crosshairs. Different image scales has been used here for better clarity. The extinction measured here is 110:1, i.e. 5.1 magnitudes (ratio between the brightest pixel of the calibration image and the brightest pixel of the FQPM image). On the "on-FQPM", one can clearly see the four lobes pattern around the center of the FQPM crosshair, as expected from the simulations (see fig. 1). It is however somewhat distorted into a diamond pattern. The right-hand image of fig. 8 shows the example of further data processing that can be applied to the "on-FQPM" images by taking advantage of the symmetry of the obtained pattern. In this case the diagonal showed as a dashed line on the center image as been used as symmetry axis, the upper-left part being subtracted from the lower-right one. The extinction after this "quadrants subtraction" is now 220:1.

Fig. 9 presents cuts on the three images, along the 45 degrees line used for quadrants subtraction, to show the PSF shape in the different cases: the solid line corresponds to the "off-FQPM" case, the dashed one to the "on-FQPM" case, and the dash-dotted line shows the result of the "quadrant-subtraction". As one can see, the quadrants subtraction improves the rejection on the max of the image, but also reduce the remaining flux in the halo.

Fig. 10 presents the same results for a binary star, HD148112. The same images as in fig. 8 are presented here. On the off-FQPM image, one can see the companion that lies between the first and second Airy rings of the bright parent star, but its parameters (flux, separation) determination is perturbed by these rings, as they have comparable flux levels. Centering the brighter star on the FQPM then allows a very clear view of its companion (in the on-FQPM image) as the flux level of the remaining light from the intrinsically brighter star is now significantly below that of the dimmer companion. The extinction ratio on the parent star was here of 80:1, i.e. 4.7 magnitudes, with the $Brackett - \gamma$ filter. The quadrant-subtracted technique allows removing only the symmetrical pattern on the image, i.e. only the light from the star in the center, leaving the companion unaffected. After quadrant-subtraction, the extinction on the flux of the parent star is 235:1, i.e. 5.9 magnitudes. The flux ratio measured here between the two stars is 23:1, and their separation is 0.730 arcsec. The diffraction limit of a 1.5 m aperture being 0.370 arcsec, this off-axis phase mask coronagraph approach has already successfully allowed imaging of a companion about $2 \times \lambda/D$ away from a star 3.5 mag brighter.

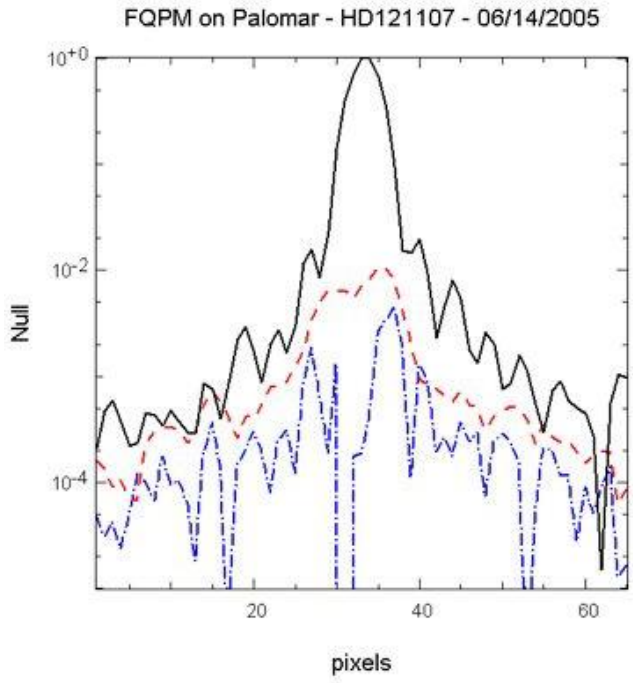

Figure 9. PSF obtained on a single star (HD121107) through the FQPM instrument. Left: off-FQPM. Center: on-FQPM. Right: on-FQPM after data processing using quadrants subtraction.

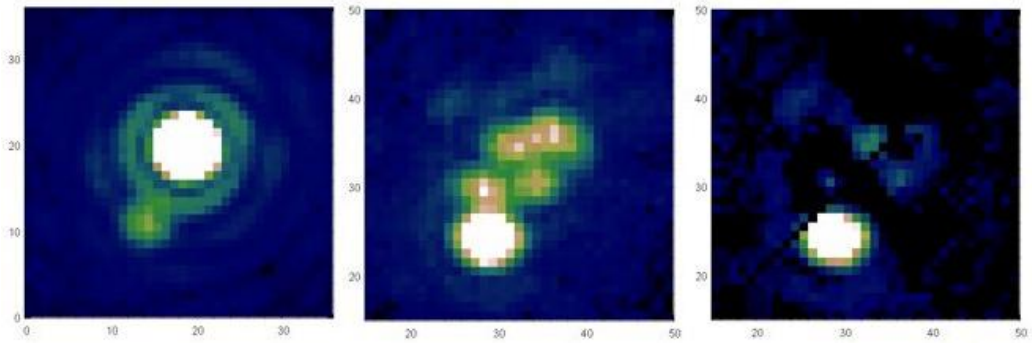

Figure 10. Image of a binary (HD148112) through the FQPM instrument. Left: image obtained off the mask (off-FQPM). Center: with the star centered on the crosshair of the mask (on-FQPM). Right: on-FQPM image after data processing using quadrants subtraction.

5. CONCLUSION

Numerical simulations have been conducted on the innovative concept of FQPM coronagraphy. These showed the possibility, with a new type of unobscured, off-axis coronagraph, to achieve a regime of increased contrast near bright stars, compared to more classical coronagraph designs.

We then designed and successfully installed our coronagraph on the Palomar 200 inches telescope (CA, USA). Our instrument has been designed as an add-on system to the Palomar Adaptive Optics (PALAO) instrument, and takes advantage of the high AO-performance level.

A first on-sky run in June 2005 has proven the very promising capabilities of this combination of off-axis telescope and coronagraphic phase mask. Extinction ratios on stars as high as 235:1, after specific data processing, have been obtained in the near-infrared with a passband of 1.3%. Detection capabilities of faint companions in the very close neighborhood of bright stars have also been demonstrated. With the experience acquired with this first on-sky run in terms of operation of this new type of coronagraph, possible improvements have been clearly identified to increase the rejection ratio and the wavelength range through mask optimization and new designs.

ACKNOWLEDGMENTS

The work presented here was conducted at the Jet Propulsion Laboratory, California Institute of Technology, under contract with the National Aeronautics and Space Administration. Observations at the Palomar Observatory were made as part of a continuing collaborative agreement between Palomar Observatory and the Jet Propulsion Laboratory. The authors wish to thank Matthew Dickie from Micro-Devices Laboratory at JPL for the manufacturing of the masks. We also wish to thank Rick Burruss and Jeff Hickey and all the staff of the Palomar 200 inches telescope for their assistance in installing and operating our instrument.

REFERENCES

[1] B. Lyot, "The study of the solar corona and prominences without eclipses", MNRAS, Volume 99, p. 580, (1939).

[2] F. Roddier, and C. Roddier, Stellar Coronograph with Phase Mask, The Publications of the Astronomical Society of the Pacific, Volume 109, pp.815-820 (1997).

[3] D. Rouan, P. Riaud, A. Boccaletti, Y. Clenet, and A. Labeyrie, The Four-Quadrant Phase-Mask Coronagraph. I. Principle, The Publications of the Astronomical Society of the Pacific, Volume 112, Issue 777, pp. 1479-1486 (2000).

[4] P. Baudoz, J. Gay, and Y. Rabbia, Achromatic interfero coronagraphy I. Theoretical capabilities for ground-based observations, Astronomy & Astrophysics Supplement, Volume 141, pp.319-329 (2000).

[5] C. Aime, R. Soummer, and A. Ferrari, Interferometric apodization of rectangular apertures. Application to stellar coronagraphy, Astronomy & Astrophysics, Volume 379, pp.697-707 (2001).

[6] D. Spergel, and J. Kasdin, A Shaped Pupil Coronagraph: A Simpler Path towards TPF, 199th American Astronomical Society Meeting, Bulletin of the AAS, Volume 33, p.1431 (2001).

[7] M.J. Kuchner, and W.A. Traub, A Coronagraph with a Band-limited Mask for Finding Terrestrial Planets, The Astrophysical Journal, Volume 570, Issue 2, pp. 900-908 (2002).

[8] O. Guyon, Phase-induced amplitude apodization of telescope pupils for extrasolar terrestrial planet imaging, Astronomy & Astrophysics, Volume 404, pp.379-387 (2003).

[9] R. Soummer, K. Dohlen, and C. Aime, Achromatic dual-zone phase mask stellar coronagraph, Astronomy & Astrophysics, Volume 403, pp.369-381 (2003).

[10] N.J. Kasdin, R.J. Vanderbei, M.G. Littman, and D.N. Spergel, Optimal one-dimensional apodizations and shaped pupils for planet finding coronagraphy, Applied Optics, Volume 44, Issue 7, pp.1117-1128 (2005).

[11] J.P. Lloyd, D.T. Gavel, J.R Graham, P.E. Hodge, A. Sivaramakrishnan, and G.M. Voit, Four-quadrant phase mask coronagraph: analytical calculation and pupil geometry, Proc. SPIE, Volume 4860, pp. 171-181 (2003).

[12] P. Riaud, A. Boccaletti, D. Rouan, F. Lemarquis, and A. Labeyrie, The Four-Quadrant Phase-Mask Coronagraph. II. Simulations, The Publications of the Astronomical Society of the Pacific, Volume 113, Issue 787, pp. 1145-1154 (2001).

[13] P. Riaud, A. Boccaletti, J. Baudrand, and D. Rouan, The Four-Quadrant Phase Mask Coronagraph. III. Laboratory Performance, The Publications of the Astronomical Society of the Pacific, Volume 115, Issue 808, pp. 712-719 (2003).

[14] A. Boccaletti, P. Riaud, P. Baudoz, J. Baudrand, D. Rouan, D. Gratadour, F. Lacombe, and A.-M. Lagrange, The Four-Quadrant Phase Mask Coronagraph. IV. First Light at the Very Large Telescope, The Publications of the Astronomical Society of the Pacific, Volume 116, Issue 825, pp. 1061-1071 (2004).

[15] P. Haguenauer, E. Serabyn, E. E. Bloemhof, J. K. Wallace, R. O. Gappinger, B. P. Mennesson, M. Troy, C. D. Koresko, J. D. Moore, "An off-axis four-quadrant phase-mask coronagraph for Palomar: high contrast near bright stars imager", Proc. SPIE, Volume 5905, pp. 261-271 (2005).

[16] G. Serabyn, P. Haguenauer, C. Koresko, An off-axis coronagraph for near neighbor detection, (in preparation).

[17] M. Troy, R. Dekany, G. Brack, B. Oppenheimer, E. Bloemhof, T. Trinh, F. Dekens, F. Shi, T. Hayward, and B. Brandl, Palomar adaptive optics project: status and performances, Proc. SPIE, Volume 4007, pp. 31-40 (2000).